Article

Long-Range Electronic Coupling of MM Quadruple Bonds (M = Mo or W) via a 2,6-Azulenedicarboxylate Bridge

Mikhail V. Barybin, Malcolm H. Chisholm, Naresh S. Dalal, Thomas H. Holovics, Nathan J. Patmore, Randall E. Robinson, and David J. Zipse

J. Am. Chem. Soc., **2005**, 127 (43), 15182-15190• DOI: 10.1021/ja0541884 • Publication Date (Web): 08 October 2005

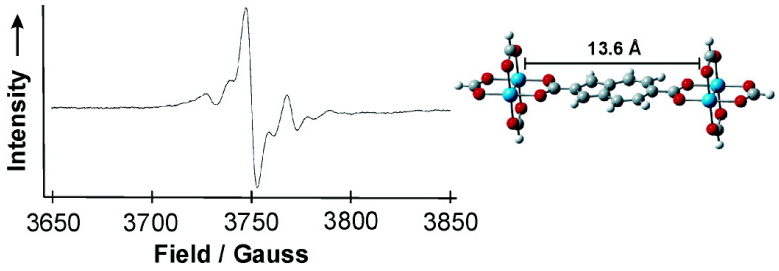

More About This Article

Additional resources and features associated with this article are available within the HTML version:

- Supporting Information
- Links to the 5 articles that cite this article, as of the time of this article download
- Access to high resolution figures
- Links to articles and content related to this article
- Copyright permission to reproduce figures and/or text from this article

View the Full Text HTML

J|A|C|S
ARTICLES
Published on Web 10/08/2005

Long-Range Electronic Coupling of MM Quadruple Bonds (M = Mo or W) via a 2,6-Azulenedicarboxylate Bridge

Mikhail V. Barybin,*,† Malcolm H. Chisholm,*,‡ Naresh S. Dalal,*,§ Thomas H. Holovics,† Nathan J. Patmore,‡ Randall E. Robinson,† and David J. Zipse§

Contribution from the Department of Chemistry, The University of Kansas, 1251 Wescoe Hall Drive, Lawrence, Kansas 66045-7582, Department of Chemistry, The Ohio State University, 100 West 18th Avenue, Columbus, Ohio 43210-1185, and Department of Chemistry and Biochemistry, National High Magnetic Field Laboratory, Florida State University, Tallahassee, Florida 32306

Received June 24, 2005; E-mail: chisholm@chemistry.ohio-state.edu

Abstract: The preparation of 2,6-azulenedicarboxylic acid (**I**) from its diester, 2-$CO_2{}^tBu$-6-CO_2-$C_{10}H_6$ (**II**), is reported together with the crystal and molecular structure of the ester, **II**. From the reactions between the dicarboxylic acid **I** and the MM quadruply bonded complexes $M_2(O_2C{}^tBu)_4$, where M = Mo or W, the azulenedicarboxylate bridged complexes $[M_2(O_2C{}^tBu)_3]_2(\mu$-2,6-$(CO_2)_2-C_{10}H_6)$ have been isolated, **III** (M = Mo) and **IV** (M = W). The latter compounds provide examples of electronically coupled M_2 centers via a polar bridge. The compounds show intense electronic absorptions due to metal-to-bridge charge transfer. This occurs in the visible region of the spectrum for **III** (M = Mo) but in the near-IR for **IV** (M = W). One electron oxidation with $Ag^+PF_6^-$ in THF generates the radical cations $\mathbf{III}^+$ and $\mathbf{IV}^+$. By both UV−vis−NIR and EPR spectroscopy the molybdenum ion $\mathbf{III}^+$ is shown to be valence trapped or Class II on the Robin and Day classification scheme. Electrochemical, UV−vis−NIR, and EPR spectroscopic data indicate that, in the tungsten complex ion $\mathbf{IV}^+$, the single electron is delocalized over the two W_2 centers that are separated by a distance of ca. 13.6 Å. Furthermore, from the hyperfine coupling to ^{183}W ($I = {}^1/_2$), the singly occupied highest molecular orbital is seen to be polarized toward one W_2 center in relationship to the other. Electronic structure calculations employing density functional theory indicate that the HOMO in compounds **III** and **IV** is an admixture of the two M_2 δ orbitals that is largely centered on the M_2 unit having proximity to the C_5 ring of the azulenedicarboxylate bridge. The energy of the highest occupied orbital of the bridge lies very close in energy to the M_2 δ orbitals. However, this orbital does not participate in electronic coupling by a hole transfer superexchange mechanism, and the electronic coupling in the radical cations of **III** and **IV** occurs by electron transfer through the bridge π^* system.

Introduction

Electron transfer processes permeate virtually all aspects of chemical, physical, and biological sciences.[1] The terms *electron* or *hole transfer* and *hopping* are commonly used but, depending upon the system under study, may take on a different meaning. Complexes containing two otherwise identical redox centers separated by a bridge constitute a unique class of materials in the study of the mechanisms involved in electronic coupling and electron/hole transfer. The redox centers may be organic or inorganic, and in this paper are two dimolybdenum or ditungsten centers each having MM quadruple bonds. As we shall show, these have particularly attractive features for the study of electronic coupling through a bridge as they are, in many ways, much more simple than the now classic example of the Creutz−Taube ion, $[(NH_3)_5Ru(\mu$-pyrazine$)Ru(NH_3)_5]^{5+}$.[2]

In a strongly coupled system, two redox centers are electronically linked through the agency of the bridging π-system such that the mixed-valence state can be diagrammatically depicted by Scheme 1. This represents the two-site super-exchange model first advanced by McConnell in 1961.[3]

The electronic coupling arises as a result of the combined efficiencies of electron transfer via the π^* system of the bridge and hole transfer by bridge π-to-metal electron transfer. Normally, one of these processes dominates, and the major contribution also involves rather specific orbitals as determined by symmetry and energy considerations. In the Robin and Day scheme,[4] a strongly coupled system is Class II and a fully delocalized one, one in which each redox center is equivalent in its oxidized (or reduced) state, is Class III. Recently, considerable attention has been devoted to compounds on the Class II/III border in both inorganic and organic systems.[5,6]

† The University of Kansas.
‡ The Ohio State University.
§ Florida State University.

(1) (a) Huynh, M. H. V.; Dattelbaum, D. M.; Meyer, T. J. *Coord. Chem. Rev.* **2005**, *249*, 457. (b) Lewis, F. D.; Letsinger, R. L.; Wasielewski, M. R. *Acc. Chem. Res.* **2001**, *34*, 159. (c) Beratan, D. N.; Onuchic, J. N.; Winkler, J. R.; Gray, H. B. *Science* **1992**, *258*, 1740. (d) Jortner, J.; Bixon, M.; Langenbacher, T.; Michel-Beyerle, M. E. *Proc. Natl. Acad. Sci. U.S.A.* **1998**, *95*, 12759.
(2) Creutz, C.; Taube, H. *J. Am. Chem. Soc.* **1968**, *91*, 3988.
(3) McConnell, H. M. *J. Chem. Phys.* **1961**, *35*, 508.
(4) Robin, M. B.; Day, P. *Adv. Inorg. Radiochem.* **1967**, *10*, 247.

10.1021/ja0541884 CCC: $30.25

Scheme 1

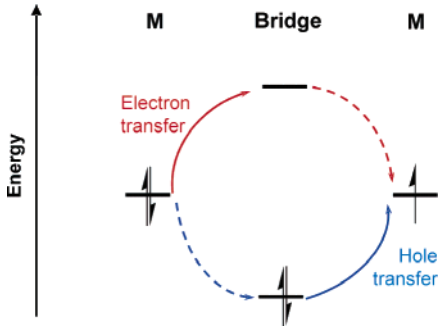

Scheme 2

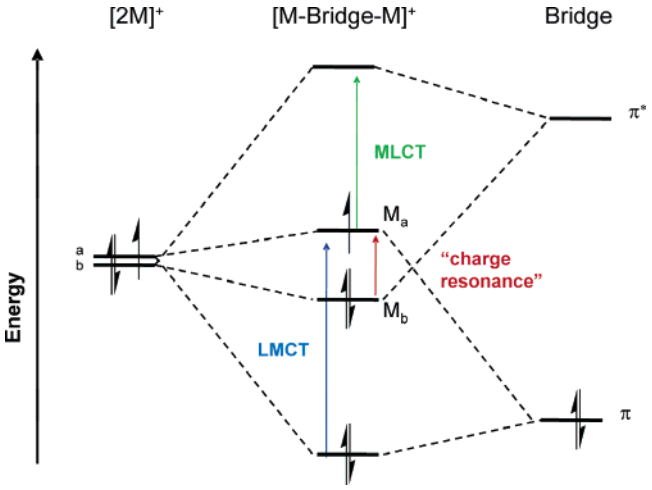

A Class III system is best described by a molecular orbital approach and is shown in a simplified form by the diagram in Scheme 2 that represents a generic system in which two metal centers are bridged by an organic linker. The in-phase and out-of-phase metal d_π combinations find a match with ligand filled and empty π-orbitals. These interactions give rise to a splitting of the metal d_π orbitals; one is stabilized by back-bonding to the bridge π^*, and the other is destabilized by a filled−filled π-interaction. As depicted in Scheme 2, the HOMO and HOMO-1 can be considered to be predominantly metal-based but with some bridge character.

The electronic transitions that arise are commonly classified as (i) the charge resonance absorption, (ii) MLCT, and (iii) LMCT, and their origin can be traced to the simple orbital splitting diagram shown in Scheme 2. The terms IVCT and MMCT are often carried over from the Class II systems but are not rigorously appropriate in a fully delocalized system. The HOMO-1→HOMO transition involves metal-based orbitals that are bonding and antibonding with respect to the bridge π-orbitals. For a symmetrical Class III system the term "charge resonance absorption" is more suitable.[7] The other absorptions, referred to as MLCT and LMCT, remain appropriate for a Class III compound, and the diagram shown in Scheme 2 is well suited for the system at hand. The Ru^{II} bridge-Ru^{III} and related t_{2g}^6-bridge-t_{2g}^5 systems are much more complex as a result of the presence of three metal d_π orbitals (d_{xy}, d_{xz}, and d_{yz}) and spin−orbit coupling which give rise to several electronic transitions in the low energy region.[5] The energy of the electronic transition involving the HOMO and HOMO-1 in Scheme 2 simply corresponds to $2H_{ab}$ for a Class III system, where H_{ab} (sometimes variously referred to as V_{ab}) is a direct measure of the strength of the electronic coupling of the two metal centers. The magnitude of H_{ab} is well documented to decrease with increasing separation of the redox-active metal centers,[8,9] and as was recently noted by Launay,[10] there are very few examples of Class III behavior beyond a distance of 10 Å, although some electronic coupling, Class II behavior has been noted at distances of 25 Å.[11]

We describe in this paper the synthesis of 2,6-azulenedicarboxylic acid, together with the preparation and characterization of M_2 quadruply bonded complexes of molybdenum and tungsten linked through the agency of the 2,6-azulenedicarboxylate bridge. This work follows on from earlier work in our laboratory[12−15] and that of Cotton and Murillo[16] involving dicarboxylate-bridged dinuclear species. This work, however, is particularly interesting and unusual because of the following: (1) The 2,6-azulenedicarboxylate bridge is polar due to the permanent dipole of about 1 D[17] associated with the resonance form of the azulenic framework, shown in structure **A** below. The importance of this ionic contribution is, however, expected to be small, as full-blown charges of + and − one electron at a distance of ~2.5 Å, the C_5 to C_7 centroid to centroid distance, would produce a dipole moment of 12.0 D!

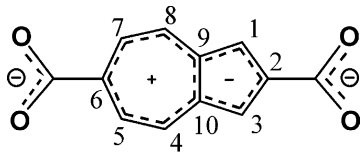

A

(2) The expected small electron−electron correlation energy[18] of this nonbenzenoid linker leads to a rather narrow HOMO−LUMO gap; thus, as is evident from Schemes 1 and 2, strong

(5) Demadis, K. D.; Hartshorn, C. M.; Meyer, T. J. *Chem. Rev.* **2001**, *101*, 2655.
(6) (a) Nelson, S. F. *Chem.—Eur. J.* **2000**, *6*, 581. (b) Brunschwig, B. S.; Creutz, C.; Sutin, N. *Chem. Soc. Rev.* **2002**, *31*, 168.
(7) Szeghalmi, A. V., et al. *J. Am. Chem. Soc.* **2004**, *126*, 7834.
(8) Ward, M. D. *Chem. Soc. Rev.* **1995**, *24*, 121.
(9) Lambert, C.; Noll, G. *J. Am. Chem. Soc.* **1999**, *121*, 8434.
(10) Launay, J.-P. *Chem. Soc. Rev.* **2001**, *30*, 386.
(11) (a) Rigaut, S.; Costuas, K.; Touchard, D.; Saillard, J.-Y.; Golhen, S.; Dixneuf, P. H. *J. Am. Chem. Soc.* **2004**, *126*, 4072. (b) Jones, S. C.; Coropceanu, V.; Barlow, S.; Kinnibrugh, T.; Timofeeva, T.; Bredas, J.-L.; Marder, S. *J. Am. Chem. Soc.* **2004**, *126*, 11782. (c) Xu, G.-L.; DeRosa, M. C.; Crutchley, R. J.; Ren, T. *J. Am. Chem. Soc.* **2004**, *126*, 3728.
(12) Cayton, R. H.; Chisholm, M. H.; Huffman, J. C.; Lobkovsky, E. B. *J. Am. Chem. Soc.* **1991**, *113*, 8709.
(13) Bursten, B. E.; Chisholm, M. H.; Clark, R. J. H.; Firth, S.; Hadad, C. M.; MacIntosh, A. M.; Wilson, P. J.; Woodward, P. M.; Zaleski, J. M. *J. Am. Chem. Soc.* **2002**, *124*, 3050.
(14) Bursten, B. E.; Chisholm, M. H.; Clark, R. J. H.; Firth, S.; Hadad, C. M.; Wilson, P. J.; Woodward, P. M.; Zaleski, J. M. *J. Am. Chem. Soc.* **2002**, *124*, 12244.
(15) (a) Chisholm, M. H. *J. Chem. Soc., Dalton Trans.* **2003**, 3821. (b) Byrnes, M. J.; Chisholm, M. H.; Clark, R. J. H.; Gallucci, J. C.; Hadad, C. M.; Patmore, N. J. *Inorg. Chem.* **2004**, *43*, 6334.
(16) (a) Cotton, F. A.; Lin, C.; Murillo, C. A. *Acc. Chem. Res.* **2001**, *34*, 759. (b) Cotton, F. A.; Lin, C.; Murillo, C. A. *Proc. Natl. Acad. Sci. U.S.A.* **2002**, *99*, 4810.
(17) (a) Robinson, R. E.; Holovics, T. C.; Deplazes, S. F.; Lushington, G. H.; Powell, D. R.; Barybin, M. V. *J. Am. Chem. Soc.* **2003**, *125*, 4432. (b) Anderson, A. G., Jr.; Steckler, B. M. *J. Am. Chem. Soc.* **1959**, *81*, 4941. (c) Robinson, R. E.; Holovics, T. C.; Deplazes, S. F.; Powell, D. R.; Lushington, G. H.; Thompson, W. H.; Barybin, M. V. *Organometallics* **2005**, *24*, 2386.
(18) (a) For a qualitative account of this phenomenon, see: Liu, R. S. H. *J. Chem. Educ.* **2002**, *79*, 183. (b) Shevyakov, S. V.; Li, H.; Muthyala, R.; Asato, A. E.; Croney, J. C.; Jameson, D. M.; Liu, R. S. H. *J. Phys. Chem. A* **2003**, *107*, 3295.

coupling might be expected as a result of the similar energy of the metal and bridge-based orbitals. From energy considerations alone, one might expect the participation of both electron and hole transfer in the super-exchange mechanism, and in the molecular orbital description, we might anticipate the possibility of a significant mixing of metal and bridge π-orbitals in both the HOMO and HOMO-1. (3) The separation of the two dinuclear centers by nearly 14 Å clearly places these complexes in the long-range category, and the comparison of molybdenum versus tungsten allows one to effectively examine just the electronic factors on the mixed valence ions, since size and solvation factors should be almost identical. As we now show, electronic factors are, indeed, remarkably important as the radical cation of the tungsten complex shows Class III behavior, while the molybdenum complex is Class II.

Experimental Section

Physical Techniques. EPR measurements were made at the Q-band (34 GHz) frequencies using a Bruker Elexsys-500 spectrometer, equipped with an ER 051 QG bridge. A built-in Bruker NMR gaussmeter and an EIP model 548 B digital frequency counter were used for accurate magnetic field and microwave frequency measurements. Variable temperatures from the ambient to 4 K were achieved using an Oxford helium flow cryostat, to an accuracy of 0.1 K. X-band EPR spectra were recorded using a Bruker ESP300 Electron Spin Resonance spectrometer. Temperature regulation was achieved by employing a Bruker Variable Temperature Unit.

UV−vis spectra of **I** were recorded using a CARY 100 spectrophotometer. UV/vis/NIR spectra of **III** and **IV** were recorded using a PerkinElmer Lambda 900 UV/vis/NIR spectrometer, with nitrogen purging. Path length IR quartz cells of 0.20, 1.00, or 10.00 mm were employed. The background spectra of the neat solvents were subtracted.

NMR samples of $\mathbf{I}H_2$ were analyzed on a Bruker DRX-400 spectrometer. The ^{1}H NMR spectra of **III** and **IV** were recorded on a 400 MHz Bruker DPX Avance spectrometer. ^{1}H and ^{13}C chemical shifts are given with reference to residual ^{1}H and ^{13}C solvent resonances relative to $SiMe_4$. Two-dimensional NMR techniques (^{1}H−^{13}C HMQC, and ^{1}H−^{13}C HMBC)[19] were employed to obtain unambiguous assignments of ^{1}H and ^{13}C NMR resonances. The aromatic hydrogen resonances are labeled in reference to the corresponding carbon atoms of the azulene framework.

The cyclic voltammograms and differential pulse voltammograms of **III** and **IV** were collected at scan rates of 100 mV s^{-1} and 5 mV s^{-1}, respectively, using a Princeton Applied Research (PAR) 173A potentiostat-galvanostat equipped with a PAR 176 current-to-voltage converter. Electrochemical measurements were performed under an inert atmosphere in a 0.1 M solution of ^{n}Bu$_4$NPF$_6$ in THF inside a single-compartment voltammetric cell equipped with a platinum working electrode, a platinum wire auxiliary electrode, and a pseudo-reference electrode consisting of a silver wire in 0.1 M ^{n}Bu$_4$NPF$_6$/THF separated from the bulk solution by a Vycor tip. The potentials are referenced internally to the $FeCp_2/FeCp_2^+$ couple by adding of a small amount of $FeCp_2$ to the solutions of the complexes.

Microanalysis was performed by Atlantic Microlab, Inc. (**III** and **IV**) and Desert Analytics ($\mathbf{I}H_2$).

Matrix assisted laser desorption/ionization time-of-flight (MALDI-TOF) was performed on a Bruker Reflex III (Bruker, Breman, Germany) mass spectrometer operated in linear, positive ion mode with an N2 laser. Laser power was used at the threshold level required to generate signal. Accelerating voltage was set to 28 kV. Dithranol was used as the matrix and prepared as a saturated solution in THF. Allotments of matrix and sample were thoroughly mixed together; 0.5 mL of this was spotted on the target plate and allowed to dry.

Synthetic Work. All manipulations of dimolybdenum or ditungsten compounds were performed in a nitrogen-filled glovebox or by using standard Schlenk line techniques. All solvents were dried using standard procedures and degassed prior to use. $Mo_2(O_2C^tBu)_4$[20] and $W_2(O_2C^t$-$Bu)_4$[21] were synthesized according to previously published literature procedures. 2-*tert*-Butoxycarbonyl-6-ethoxycarbonyl-azulene (**II**) and 2-*tert*-butoxycarbonyl-6-azulenecarboxylic acid were prepared from 2-indanecarboxylic acid[22] via a modified procedure of Lightner *et al*.[23] $\mathbf{III}^+PF_6^-$ and $\mathbf{IV}^+PF_6^-$ were generated in situ prior to UV/vis/NIR and EPR spectroscopy measurements due to their instability,[24,25] by treatment of **III** and **IV** with 1 equiv of $AgPF_6$ in THF.

2,6-Azulenedicarboxylic Acid ($\mathbf{I}H_2$). A pine green sample of 2-*tert*-butoxycarbonyl-6-azulenecarboxylic acid (0.250 g, 0.918 mmol) was treated with 20 mL of formic acid. The mixture was stirred at ambient temperature for 5 h. Then, the volatiles were removed at 10^{-2} Torr. The residue was dried at 40 °C and 10^{-2} Torr for 6 h to afford 2,6-azulenedicarboxylic acid (0.195 g, 0.902 mmol) as a finely divided, dark chocolate-brown powder in a 98% yield. The product does not melt up to 400 °C. The diacid $\mathbf{I}H_2$ is extremely hygroscopic and strongly holds onto water. Anal. Calcd for $C_{12}H_8O_4\cdot(H_2O)_{0.235}$: C, 65.39; H, 3.87. Found: C, 65.38; H, 3.87. ^{1}H NMR (DMSO-d_6, 400 MHz, 22 °C): δ13.32 (br s, 2H, CO_2H), 8.67 (d, 2H, J = 9.9 Hz, $H^{4,8}$); 8.01 (d, 2H, J = 9.9 Hz, $H^{5,7}$); 7.80 (s, 2H, $H^{1,3}$) ppm. ^{13}C NMR (DMSO-d_6, 100.6 MHz, 22 °C): δ 168.7 (C^6CO_2H), 166.2 (C^2CO_2H), 141.4 (C^6), 140.6 ($C^{4,8}$), 139.9 (C^2), 139.4 ($C^{9,10}$), 124.0 ($C^{5,7}$), 119.3 ($C^{1,3}$) ppm. UV−vis (in 0.034 M aqueous KOH, 295 K, values of $\epsilon \times 10^{-3}$ are given in parentheses): 622 br (0.42), 364 (11.44), 349 (5.26), 336 (3.71), 295 sh (51.65), 289 (66.39) nm.

[(^{t}BuCO$_2$)$_3$Mo$_2$]$_2$(μ-O$_2$CC$_{10}$H$_6$CO$_2$) (III). A Schlenk tube was charged with $Mo_2(O_2C^tBu)_4$ (0.350 g, 0.587 mmol) and $\mathbf{I}H_2$ (0.063 g, 0.291 mmol). Toluene (10 mL) was added, and the suspension was stirred for 8 days, during which time a blue precipitate formed. The microcrystalline product was isolated by centrifugation and washed with toluene (1 × 15 mL) and hexanes (1 × 15 mL). The solid was dried in vacuo to give 0.240 g (68% yield) of blue **III**. Anal. Calcd For $C_{42}H_{60}O_{16}Mo_4$: C, 41.87; H, 5.02. Found: C, 42.04; H, 4.94. ^{1}H NMR-(THF-d_8, 400 MHz): δ 8.48 (d, 2H, J_{HH} = 10.8 Hz), 8.40 (d, 2H, J_{HH} = 10.8 Hz), 7.90 (s, 2H), 1.45 (s, 9H + 9H coincidence), 1.40 (s, 18H), 1.38 (s, 18H) ppm. MALDI-TOF: Calcd monoisotopic mw for $C_{42}H_{60}O_{16}Mo_4$: 1212.010 (M^+). Found: 1212.553. UV−vis−NIR (in THF, 293 K, values of $\epsilon \times 10^{-3}$ are given in parentheses): 709 br (38.52), 330 sh (19.13), 291 (49.22), 215 (16.66) nm.

[(^{t}BuCO$_2$)$_3$W$_2$]$_2$(μ-O$_2$CC$_{10}$H$_6$CO$_2$) (IV). A Schlenk tube was charged with $W_2(O_2C^tBu)_4$ (0.215 g, 0.278 mmol) and 2,6-azulenedicarboxylate (0.030 g, 0.139 mmol). Toluene (10 mL) was added, and the suspension was stirred for 8 days, during which time a pale green precipitate formed. The microcrystalline product was isolated by centrifugation and washed with toluene (2 × 15 mL) and hexanes (1 × 15 mL). The solid was dried in vacuo to give 0.116 g (54% yield) of pale green **IV**. ^{1}H NMR (THF-d_8, 400 MHz): δ 7.82 (d, 2H, J_{HH} = 11.2 Hz), 7.32 (s, 2H), 7.30 (d, 2H, J_{HH} = 11.2 Hz), 1.43 (s, 9H), 1.42 (s, 9H), 1.35 (s, 18H), 1.34 (s, 18H) ppm. MALDI-TOF: Calcd monoisotopic mw for $C_{42}H_{60}O_{16}W_4$: 1556.329 (M^+). Found: 1556.516. UV−vis−NIR (in THF, 293 K, values of $\epsilon \times 10^{-3}$ are given in parentheses): 1145 (85.83), 969 sh (29.02), 373 (22.39), 273 (34.99) nm.

(19) Levitt, M. H. *Spin Dynamics. Basics of Nuclear Magnetic Resonance.* John Wiley & Sons: New York, 2001.

(20) Brignole, A. B.; Cotton, F. A. *Inorg. Synth.* **1971**, *13*, 81.
(21) Santure, D. J.; Huffman, J. C.; Sattelberger, A. P. *Inorg. Chem.* **1985**, *24*, 371.
(22) Carlson, G. L. B.; Quina, F. H.; Zarnegar, B. M.; Whitten, D. G. *J. Am. Chem. Soc.* **1975**, *97*, 347.
(23) Zindel, J.; Maitra, S.; Lightner, D. A. *Synthesis* **1996**, 1217.
(24) Chisholm, M. H.; Pate, B. D.; Wilson, P. J.; Zaleski, J. M. *Chem. Commun.* **2002**, 1084.
(25) Chisholm, M. H.; Clark, R. J. H.; Gallucci, J. C.; Hadad, C. M.; Patmore, N. J. *J. Am. Chem. Soc.* **2004**, *126*, 8303.

Table 1. Crystal Data, Data Collection, Solution, and Refinement for **II**

empirical formula	$C_{18}H_{20}O_4$
formula weight	300.34
crystal habit, color	plate, green
crystal size (mm^3)	0.41 × 0.18 × 0.02
crystal system	monoclinic
space group	$P2_1/c$
a (Å)	6.575(4)
b (Å)	34.86(2)
c (Å)	6.896(4)
α (deg)	90
β (deg)	96.310(16)
γ (deg)	111.283(2)
V (Å^3)	1571.0(17)
Z, Z'	4, 1
ρ_{calc} (Mg m^{-3})	1.270
μ (mm^{-1})	0.089
F(000)	640
temp (K)	100(2)
θ range (deg)	3.03−26.00
rflns collected	16984
max/min transmission	0.998/0.964
data/restraints/params	16984/71/229
rflns with $I > 2\sigma(I)$	9728
$R1^a$; $wR2^b$	0.0689; 0.1956
GOF on F^2	1.001
largest diff peak/hole (e·Å^{-3})	0.861/−0.285

[a] $R1 = \sum||F_o| - |F_c||/\sum|F_o|$. [b] $wR2 = [\sum(w(F_o^2 - F_c^2)^2)/\sum(w(F_o^2)^2)]^{1/2}$.

Electronic Structure Calculations. Electronic structure calculations on the model compounds $[(HCO_2)_3M_2]_2(\mu\text{-}O_2CC_{10}H_6CO_2)$ (M = Mo, W) were performed using density functional theory with the aid of the Gaussian03 suite of programs.[26] The B3LYP functional[27,28] along with the 6-31G* (5d) basis set[29] was used for H, C, O, and N along with the SDD energy consistent pseudopotentials for molybdenum and tungsten.[30] Geometry optimizations were performed in C_{2v} symmetry and confirmed as local minima on the potential energy surfaces using frequency analysis.

X-ray Work. X-ray quality crystals of 2-*tert*-butoxycarbonyl-6-ethoxycarbonyl-azulene[23] (**II**) were grown by slow evaporation of its heptane solution at 22 °C. The selected crystal was twinned by a 2-fold rotation about the [001] plane. Intensity data were collected using a Bruker APEX CCD area detector mounted on a Bruker D8 goniometer. Graphite-monochromated Mo Kα radiation (λ = 0.710 73 Å) was employed. The data were corrected for absorption by a semiempirical method.[31] The monoclinic space group $P2_1/c$ was determined by statistical tests and verified by subsequent refinement. The structure was solved by direct methods and refined by full-matrix least-squares methods on F^2. Hydrogen atom positions were initially determined by geometry and refined by a riding model. Non-hydrogen atoms were refined with anisotropic displacement parameters. Hydrogen atom displacement parameters were set to 1.2 (1.5 for methyl) times the displacement parameters of the bonded atoms. Restraints were applied to the disordered end of the molecule (O2, C11, and C12). All calculations employed the SHELXTL V5.0 suite of programs (SHELXTL-Plus V5.0, Siemens Industrial Automation, Inc, Madison, Wisconsin). Crystal data, data collection, solution, and refinement information for **II** are summarized in Table 1. A full description of the crystallographic work is available in the Supporting Information. All anisotropic displacement parameters are drawn at the 50% probability level.

Scheme 3

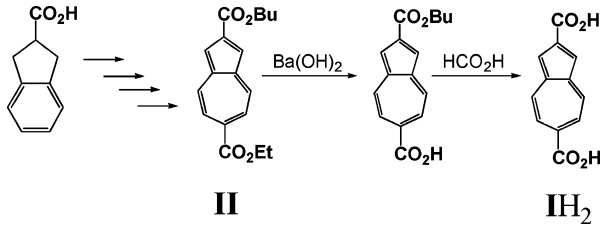

Results and Discussion

2,6-Azulenedicarboxylate Framework and 2,6-Azulenedicarboxylic Acid. In their investigation of synthetic routes to 2,6-substituted "push−pull" azulenes, Lightner and co-workers[23] developed an elegant four-step assembly of 2-*tert*-butoxycarbonyl-6-ethoxycarbonyl-azulene (**II**) from 2-indane and showed that hydrolysis of **II** with $Ba(OH)_2$ in $EtOH/H_2O$ involved exclusively the ethoxycarbonyl substituent. Our treatment of pine-green-colored 2-*tert*-butoxycarbonyl-6-azulenecarboxylic acid with excess neat formic acid afforded dark chocolate-brown 2,6-azulenedicarboxylic acid (**I**H_2) in an essentially quantitative yield (Scheme 3). Diacid **I**H_2 must be stored under moisture-free conditions, as it is extremely hygroscopic and strongly holds onto water.

Compound **I**H_2 dissolves in DMSO and aqueous KOH to give deep blue solutions. In addition to three resonances of equal intensity from the azulenic H-nuclei, the ^{1}H NMR spectrum of **I**H_2 in anhydrous DMSO-d_6 features a somewhat broad signal at 13.32 ppm of the same intensity due to both acidic hydrogen atoms. The λ_{max} value of the $S_0 \rightarrow S_1$ electronic transition (HOMO→LUMO) observed for azulene dicarboxylate **I** in basic H_2O occurs at 622 nm ($\epsilon \approx 420$ M^{-1} cm^{-1}). The bathochromic shift of this band relative to the corresponding transition in azulene ($^1A \rightarrow {}^1L_b$), which occurs at λ_{max} = 577 nm in EtOH,[32] is consistent with the expectation that substitution of the azulenic nucleus with an unsaturated electron-withdrawing group at an even-numbered position should lead to stabilization of its LUMO through both conjugation and inductive effects while not significantly affecting the HOMO level.[18,32]

While attempts to obtain X-ray quality crystals of **I**H_2 invariably produced powdered samples, we were successful in crystallographic analysis of its diester precursor **II**. The molecular structure of **II** is shown in Figure 1. As in azulene itself,[33] the peripheral C−C distances within the azulenic nucleus of **II** do not exhibit significant alternation and are ca. 0.1 Å shorter than the C−C bond at the ring junction. The π-system of **II**'s *tert*-butoxycarbonyl substituent is virtually parallel to that of the azulenic framework (torsion angle O3−C18−C2−C3 = 4.7(2)°), while the carboxylate unit of the disordered ethoxycarbonyl group shows only minor deviation from coplanarity with the azulenic scaffold (torsion angle O1−C17−C6−C5 = 19.2(2)°). In addition, the solid-state structure of **II** features face-to-face π-stacking interactions between azulenic seven-membered rings with a centroid−centroid separation of 3.472 Å (see Supporting Information).

(26) Frisch, M. J., et al. *Gaussian 03*, revision B.04; Gaussian, Inc.: Pittsburgh, PA, 2003.
(27) Becke, A. D. *Phys. Rev. A* **1988**, *38*, 3098. Becke, A. D. *J. Chem. Phys.* **1993**, *98*, 5648.
(28) Lee, C.; Yang, W.; Parr, R. G. *Phys. Rev. B* **1988**, *37*, 785.
(29) Hehre, W. J.; Radom, L.; Schleyer, P. v. R.; Pople, J. A. *Ab initio Molecular Orbital Theory*; John Wiley & Sons: New York, 1986.
(30) Andrae, D.; Haeussermann, U.; Dolg, M.; Stoll, H.; Preuss, H. *Theor. Chim. Acta* **1990**, *77*, 123.
(31) Sheldrick, G. M. *Program for Empirical Absorption Correction of Area Detector*; University of Gottingen: Germany, 2000.
(32) Heilbronner, E. *Non-Benzenoid Aromatic Compounds*; Interscience Publishers: New York, 1959; p 171.
(33) Hanson, A. W. *Acta Crystallogr.* **1965**, *19*, 19.

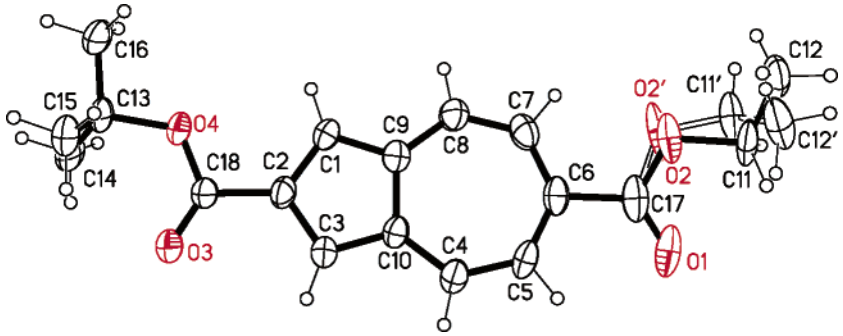

Figure 1. ORTEP diagram of 2,6-azulene diester **II**. Both modeled orientations of the disordered ethoxy group, O2−C11−C12 ($^2/_3$ occupancy) and O2′−C11′−C12′ ($^1/_3$ occupancy), are shown. Selected bond distances (Å) and angles (deg): C1−C2 = 1.400(2), C1−C9 = 1.402(2), C2−C3 = 1.392(2), C3−C10 = 1.412(2), C4−C10 = 1.392(2), C4−C5 = 1.392(2), C5−C6 = 1.376(2), C6−C7 = 1.394(2), C7−C8 = 1.390(2), C8−C9 = 1.385(2), C9−C10 = 1.479(2), C2−C18 = 1.488(2), C6−C17 = 1.512(2), C17−O1 = 1.202(2), C17−O2 = 1.334(2), C17−O2′ = 1.359(3), C18−O3 = 1.203(2), C18−O4 = 1.338(2), O1−C17−O2 = 120.5(2), O1−C17−O2′ = 129.0(2), O3−C18−O4 = 125.7(2).

Neutral Compounds: Mo_4 AZU and W_4 AZU. The new azulene-2,6-dicarboxylate-bridged compounds were prepared from the reactions between the dimetal tetrapivalates and the 2,6-azulenedicarboxylic acid in toluene according to the reaction shown in eq 1.

$$2M_2(O_2C^tBu)_4 + \underset{(\mathbf{I}H_2)}{2,6\text{-}(CO_2H)_2\text{-}C_{10}H_6} \xrightarrow[\text{toluene,}]{\text{8 days}} [(^tBuCO_2)_3M_2]_2(\mu\text{-}O_2CC_{10}H_6CO_2) + 2\ ^tBuCO_2H \quad (1)$$

M = Mo (**III**), W (**IV**)

The procedure outlined in eq 1 parallels earlier syntheses of bridged dicarboxylate compounds prepared in this laboratory.[12] The long reaction time of 8 days is to ensure complete reaction, since the azulenedicarboxylic acid is only sparingly soluble in toluene. The new compounds $[(^tBuCO_2)_3M_2]_2(\mu\text{-}O_2CC_{10}H_6CO_2)$, hereafter referred to as **III** (M = Mo) and **IV** (M = W), show molecular ions $\mathbf{III}^+$ and $\mathbf{IV}^+$ by MALDI-MS. The ^{1}H NMR spectra feature the expected resonances for the bridge protons in the aromatic region and two sets of two singlet $^tBuCO_2$ resonances, in the ratio 2:1, corresponding to *cis*- and *trans*-pivalate ligands (with respect to the bridge carboxylate) bound to the chemically inequivalent M_2 centers. Despite numerous attempts, crystals of **III** and **IV** suitable for single-crystal X-ray diffraction could not be obtained, although the products do give X-ray powder diffraction patterns,[34] as seen in the related $[(^tBuCO_2)_3M_2]_2(\mu\text{-}O_2CC_6F_4CO_2)$ species.[14] The compounds are air-sensitive and essentially insoluble in pure hydrocarbon solvents. They are soluble in the polar solvents THF and DMSO. Compound **IV** is unstable in solution and slowly decomposes in d_8-THF over a period of days to generate $W_2(O_2C^tBu)_4$ and pivalic acid, as evidenced by ^{1}H NMR spectroscopy, together with other as yet uncharacterized products.

Electronic Absorption Spectra. The molybdenum complex **III** is an intense blue color, whereas its tungsten congener, **IV**, is pale green in the solid state and straw yellow in THF solutions. The electronic spectra of the two complexes are compared in Figure 2. In both cases, the lowest energy electronic transitions are assignable to metal-to-bridge charge transfer. The greater intensity and the lower energy of the tungsten absorption bands arises from the higher orbital energy of the W_2 δ orbitals, which are typically 0.5 eV above Mo_2 δ orbitals in related complexes and the greater radial extension of the W 5d orbitals.

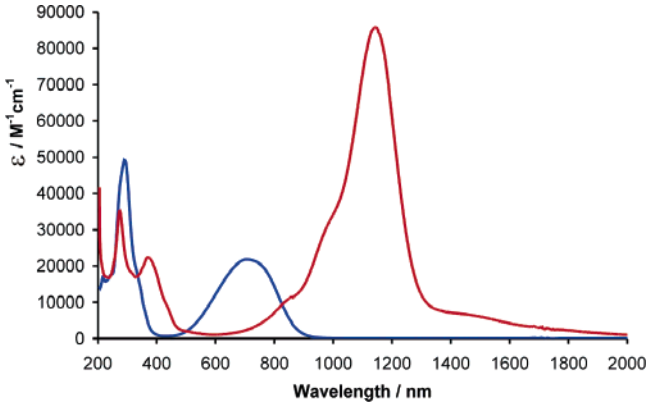

Figure 2. Electronic absorption spectra of **III** (blue) and **IV** (red) in THF at room temperature.

The latter gives rise to enhanced W_2 δ-to-bridge LUMO back-bonding. To a first-order approximation, the intensity of a MLCT band correlates with the degree of overlap and is inversely related to the orbital separation energy.

The appearance of the MLCT band in **IV** is reminiscent of that seen in the related perfluoroterephthalate bridged W_4-containing complex.[14] To lower energy of the intense (0,0) transition at 1140 nm is a broad, much weaker transition, $\epsilon \approx 8000\ M^{-1}\ cm^{-1}$, band assignable to the spin-forbidden MLCT triplet transition which gains in intensity due to spin−orbit coupling with the heavy 5d metal. The intense MLCT band at 1140 nm ($\epsilon = 85\ 700\ M^{-1}\ cm^{-1}$) has in shape a relatively sharp onset, indicative of a ground-state structure where the azulene ring and the attendant O_2C groups are in the same plane. To higher energy, there is evidence of a vibronic progression. These features are consistent with the electronic structure calculations on the model compounds described below.

The solid-state absorption spectra of **III** and **IV** as Nujol mulls are shown in the Supporting Information and are compared alongside the spectra in THF solutions. The MLCT absorptions are at a higher energy in the solid state for both **III** and **IV**, which reflects a poorer M_2 δ-bridge π overlap. Solid-state structures of related dicarboxylate bridged M_2 compounds show that intermolecular $M\cdots O_{carboxylate}$ interactions control crystal packing,[13,14] which in this instance will force the plane of the azulene bridge rings to twist with respect to the plane of the M_2 units.

Electronic Structure Calculations and Comments on Bonding. The electronic structures of **III** and **IV** were inter-

(34) Chisholm, M. H.; Mehta, A.; Patmore, N. J. Unpublished results.

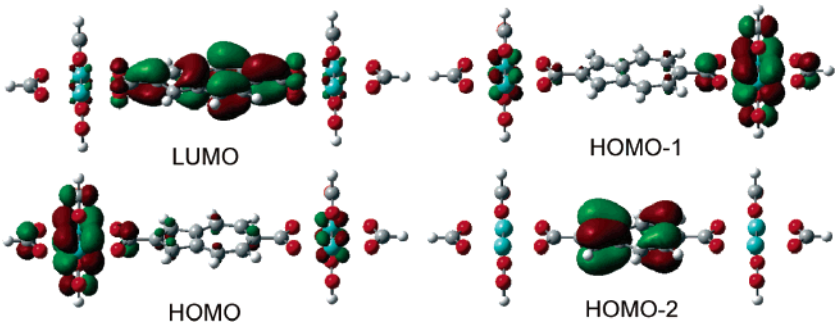

Figure 3. Selected frontier molecular orbital plots calculated for $[(HCO_2)_3Mo_2]_2(\mu\text{-}O_2CC_{10}H_6CO_2)$, with the orbitals drawn with an isosurface value of 0.03.

Table 2. Calculated Frontier MO Energies for the Model Compounds $[(HCO_2)_3W_2]_2(\mu\text{-}O_2CC_{10}H_6CO_2)$ (M = Mo, W) in C_{2v} Symmetry[a]

	$[(HCO_2)_3Mo_2]_2(\mu\text{-}O_2CC_{10}H_6CO_2)$			$[(HCO_2)_3W_2]_2(\mu\text{-}O_2CC_{10}H_6CO_2)$		
MO	eV	symmetry	assignment	eV	symmetry	assignment
LUMO+2	−2.02	a_2	δ^* A	−1.27	a_2	δ^* A
LUMO+1	−2.24	a_2	δ^* B	−1.47	a_2	δ^* B
LUMO	−3.01	b_1	bridge π^*	−2.90	b_1	bridge π^*
HOMO	−5.22	b_1	δ A	−4.70	b_1	δ A
HOMO-1	−5.53	b_1	δ B	−5.04	b_1	δ B
HOMO-2	−5.69	a_2	bridge π	−5.52	a_2	bridge π
HOMO-3	−6.91	a_1	π A	−6.21	a_1	π A
HOMO-4	−6.96	b_1	π A	−6.28	b_1	π A
HOMO-5	−7.01	b_1	bridge π	−6.41	a_1	π B
HOMO-6	−7.13	a_1	π B	−6.47	b_1	π B
HOMO-7	−7.16	a_1	σ A	−6.87	b_1	bridge π
HOMO-8	−7.17	b_1	π B	−7.22	a_1	σ A
HOMO-9	−7.37	a_1	σ B	−7.41	a_1	σ B
HOMO-10	−8.46	a_2		−8.33	a_2	bridge π

[a] Assignments "A" and "B" refer to which of the inequivalent M_2 units has the majority orbital character, as labeled in Figure 4.

rogated by employing density functional theory (DFT) calculations on the model compounds $[(HCO_2)_3M_2]_2(\mu\text{-}O_2CC_{10}H_6CO_2)$ (M = Mo, W) with the aid of the Gaussian03 suite of programs.[26] All compounds were geometry optimized in C_{2v} symmetry using the B3LYP functional[27,35] along with the 6-31G* (5d) basis set[29] for H, C, and O and using the SDD energy consistent pseudopotentials for molybdenum and tungsten.[30] See Experimental Section for further details. In the geometry optimized, ground state structures, the azulene ring is planar with respect to the M_2 units, which maximizes M_2-to-bridge π back-bonding. The structures were confirmed to be a minima on the potential energy surface by frequency analysis and yield $M_2\cdots M_2$ separations of 13.65 Å and 13.62 Å for molybdenum and tungsten, respectively.

Gaussview[36] plots of the LUMO, HOMO, HOMO-1, and HOMO-2 for $[(HCO_2)_3Mo_2]_2(\mu\text{-}O_2CC_{10}H_6CO_2)$ are shown in Figure 3. For both M = Mo and W, the HOMO and HOMO-1 are M_2 δ combinations and the LUMO is a bridge-centered π^* orbital as expected. The HOMO-2 is a bridge π-MO that is polarized toward the C_5 ring, whereas, in the LUMO, the polarization is toward the C_7 ring. Similarly, the HOMO is an M_2 δ combination having greater metal character associated with the M_2 center, which is adjacent to the C_5 ring, M_2(A), and the HOMO-1 has more character from the M_2 center adjacent to the C_7 ring, M_2(B). See Figure 4 for the M_2 labeling scheme and Table 2 for the calculated frontier molecular orbital energies. Atomic coordinates are given in the Supporting Information. The bridge-centered filled orbital, the HOMO-2, is very close

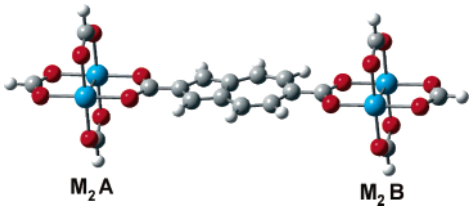

Figure 4. View of the $[(HCO_2)_3M_2]_2(\mu\text{-}O_2CC_{10}H_6CO_2)$ (M = Mo, W) model compounds. The labeling scheme for each M_2 unit either side of the polar bridge is given.

in energy to the Mo_2 δ manifold and, even for tungsten, is calculated to be only 0.5 eV below the HOMO-1 W_4 δ combination. As shown in Table 2, the M_4 π sets are well below the bridge-based HOMO-2 and do not significantly split in energy because they have little interaction with the bridging orbitals. Thus qualitatively, it is seen that the frontier orbitals of these two rather large molecules closely resemble the simple MO description represented in Scheme 2, with the exception that the metal-based orbitals are polarized.

Electrochemical Studies. Both compounds show two successive oxidation waves with the first being a reversible process on the CV time-scale. Voltammograms for **III** and **IV** are shown in Figure 5. For compound **III**, the splitting of the 1st and 2nd oxidation waves is 112 mV. This gives a comproportionation constant (K_c) of 78 for the stability of the single-oxidized radical cation in relation to the neutral and doubly oxidized compound.[37] In contrast, the tungsten complex **IV** shows two oxidation waves separated by 468 mV. This gives a value of $K_c = 8.2 \times 10^7$ which, together with the greater ease of oxidation of **IV** relative

(35) Lee, C.; Yang, W.; Parr, R. G. *Phys. Rev. B: Condens. Matter* **1988**, *37*, 785.
(36) *GaussView 3.09*; Gaussian Inc.: Pittsburgh, PA, 2003.
(37) Richardson, D. E.; Taube, H. *Inorg. Chem.* **1981**, *20*, 1278.

Table 3. Electrochemical Data and Comproportionation Constants for Selected Compounds in THF/^{n}Bu$_4$NPF$_6$ Solutions[a]

compound	$E_{1/2}^1$ (V)	$E_{1/2}^2$ (V)	$\Delta E_{1/2}$ (mV)	K_c
$Mo_2(O_2C^tBu)_4$[b]	−0.04			
$[(^tBuCO_2)_3Mo_2]_2(\mu$-$O_2CCO_2)$[b]	−0.03	+0.25	280	5.4×10^4
$[(^tBuCO_2)_3Mo_2]_2(\mu$-$O_2C-C_6F_4-CO_2)$[b]	+0.10		65	13
III	−0.09	−0.02	112	78
$W_2(O_2C^tBu)_4$[b]	−0.70			
$[(^tBuCO_2)_3W_2]_2(\mu$-$O_2CCO_2)$[b]	−1.26	−0.54	717	1.3×10^{12}
$[(^tBuCO_2)_3W_2]_2(\mu$-$O_2C-C_6F_4-CO_2)$[b]	−0.66	−0.37	285	6.6×10^4
IV	−0.91	−0.44	468	8.2×10^7

[a] Potentials are referenced to the Fc^+/Fc couple. [b] Reference 12.

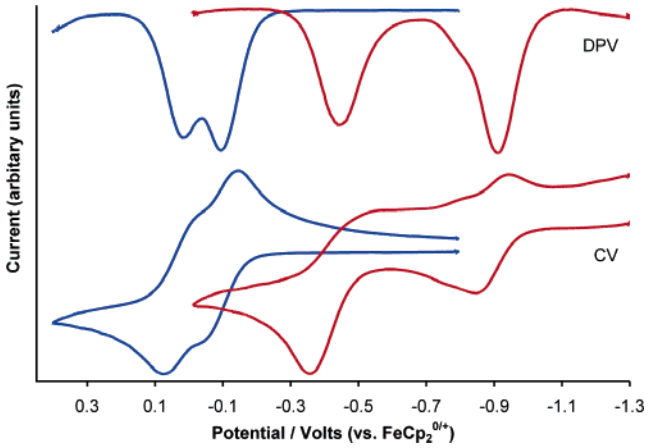

Figure 5. Cyclic voltammogram (CV) and differential pulse voltammogram (DPV) for **III** (blue) and **IV** (red) in a 0.1 M ^{n}Bu$_4$NPF$_6$/THF solution. Potentials are referenced to the $FeCp_2^{0/+}$ couple.

to $W_2(O_2C^tBu)_4$, is suggestive of Class III characteristics. The small impurity in voltammograms of **IV** at ca. −0.7 V arises from the $W_2(O_2C^tBu)_4^{0/+}$ couple because $W_2(O_2C^tBu)_4$ is formed by slow decomposition of **IV** in THF solutions. The oxidation potentials of **III** and **IV** are compared with related compounds in Table 3.

Given the asymmetric nature of the azulene bridge, the separation between successive oxidation potentials could be partially due to the different oxidation potentials of the two chemically inequivalent M_2 units, M_2(A) and M_2(B), noted above. However, we expect this effect to only contribute a small amount to the separation of the oxidation potentials and to be of the same magnitude for both Mo_2 and W_2 compounds because of their similar size and solvation. Thus the notably large $\Delta E_{1/2}$ and K_c values for the tungsten complex **IV** implicate an electronic origin and greater delocalization of the positive charge.

Electronic Absorption Spectra of III$^+$ and IV$^+$. The electronic absorption spectra of the radical cations **III**$^+$ and **IV**$^+$, generated in situ by oxidation with one equivalent of $AgPF_6$, are shown in Figures 6 and 7, respectively. They are quite different in appearance. The tungsten complex **IV**$^+$ shows an intense sharp band in the near-IR at 9260 cm^{-1} (1080 nm) and a weaker narrow band centered at 3080 cm^{-1} (3246 nm) in the infrared. The complete shape of this band is obscured by solvent absorption, but it is clearly of the type seen for Class III compounds near the Class II/III border.[6] It should be noted that this electronic transition in the IR region of the spectrum is not observed for either **IV** or **IV**$^{2+}$, though the latter species is not chemically persistent. An estimate of the peak width at half-height ($\Delta\bar{\nu}_{1/2}$) from the high energy side of the peak is 750 cm^{-1}. In a two-state classical model, the bandwidth can be calculated using $\Delta\bar{\nu}_{1/2}(\text{calcd}) = [2310\bar{\nu}_{max}]^{1/2}$ (at room temperature), which gives $\Delta\bar{\nu}_{1/2}(\text{calcd}) = 2660$ cm^{-1}. Based on the narrowness [$\Delta\bar{\nu}_{1/2}(\text{calcd}) \gg \Delta\bar{\nu}_{1/2}(\text{obsd})$] and relative intensity of this absorption, one can definitely classify this as Class III from the Hush model.[9,38] For a Class III system, the cross coupling matrix element (H_{ab}) is simply $\bar{\nu}_{max}/2$, which gives $H_{ab} = 1540$ cm^{-1} for **IV**$^+$. Based on the MO calculations on the model

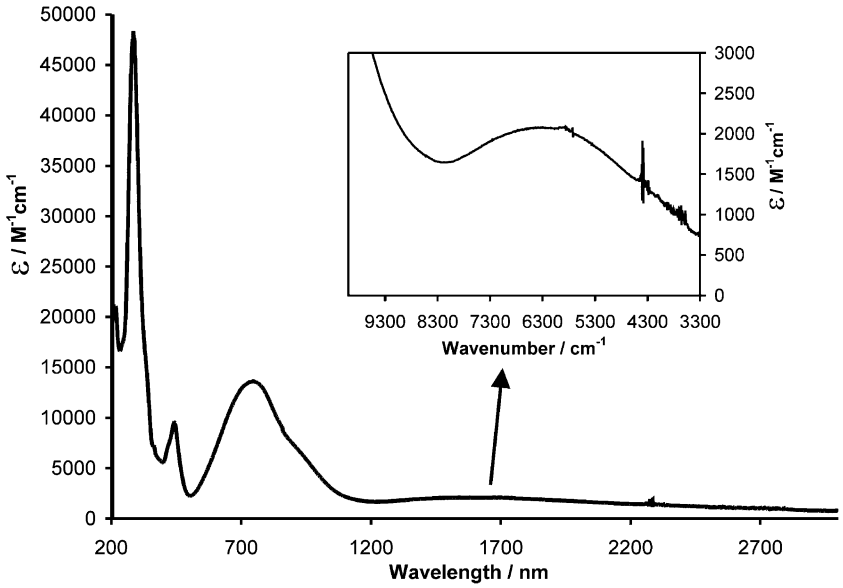

Figure 6. Electronic absorption spectrum of **III**$^+PF_6^-$ recorded in THF at 298 K. The inset shows an expansion of the IVCT absorption, plotted in wavenumbers.

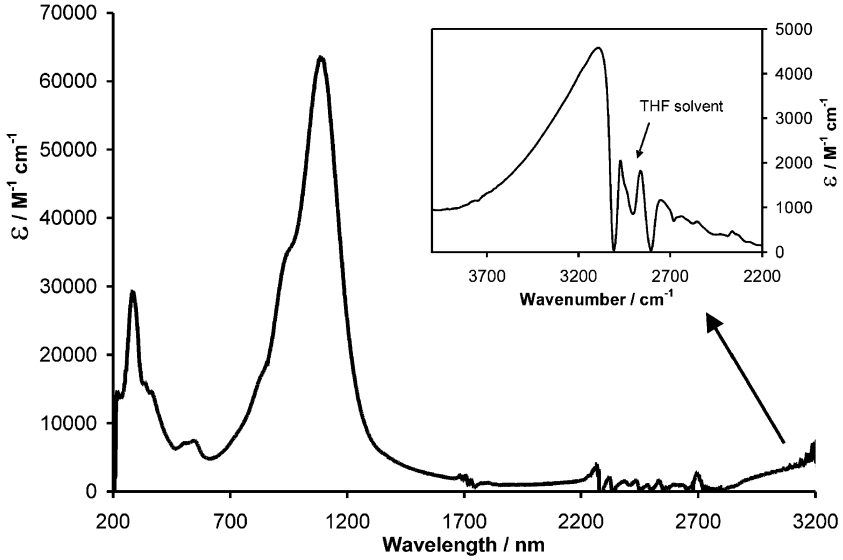

Figure 7. Electronic absorption spectrum of $\mathbf{IV}^+PF_6^-$ recorded in THF at 298 K using a UV/vis/NIR spectrometer. The inset shows an expansion of the IVCT absorption, plotted in wavenumbers, recorded using an IR spectrometer.

compounds, we can readily assign this band to originate from the HOMO-1 to HOMO transition and the higher energy band to the MLCT band. Again, this conforms to the simple picture presented in Scheme 2. No evidence of an LMCT is seen, and none is predicted in this region by time-dependent DFT calculations.

In contrast, the spectrum of $\mathbf{III}^+$ has a weak and broad low-energy band centered at 6250 cm^{-1} (1600 nm). The value of $\Delta\bar{\nu}_{1/2}$(obsd) = 4800 cm^{-1} is slightly broader than $\Delta\bar{\nu}_{1/2}$(calcd) = 3800 cm^{-1}, and this compound is best described as Class II in nature. For a Class II compound H_{ab} can be determined using $H_{ab} = (0.0206/d)(\Delta\bar{\nu}_{max}\Delta\bar{\nu}_{1/2}\epsilon_{max})^{1/2}$, where d = electron-transfer distance (Å), $\Delta\bar{\nu}_{max}$ = energy of the intervalence band (cm^{-1}) at maximum extinction coefficient, ϵ_{max} (M^{-1} cm^{-1}), and $\Delta\bar{\nu}_{1/2}$ = peak width at half peak height (cm^{-1}). The electron transfer distance (d) can be crudely estimated by using the Mo_2 unit separation from the calculated structure [Mo_2(A)−Mo_2(B) = 13.65 Å], which gives H_{ab} = 380 cm^{-1} for $\mathbf{III}^+$.

The radical cations slowly decompose in solution, and for a 10^{-4} M solution, the $t_{1/2}$ of $\mathbf{III}^+$ PF_6^- is around 1 day and, for $\mathbf{IV}^+PF_6^-$, 4 days at room temperature.

EPR Spectra of $\mathbf{III}^+$ and $\mathbf{IV}^+$ in 2⁻MeTHF. The EPR spectra of the radical cations $\mathbf{III}^+$ and $\mathbf{IV}^+$, prepared in situ by reaction with 1 equiv of $AgPF_6$ in THF, were recorded at X-band and Q-band. The Q-band spectrum of $\mathbf{III}^+$ is given in the Supporting Information and shows one species with g = 1.931. The intensity and magnitude of hyperfine coupling to ^{95}Mo and ^{97}Mo nuclei [I = 5/2, Σ_{abund} = 25.4%], A_0 = 27 G, indicate that the radical cation is valence-trapped with the unpaired electron localized on one Mo_2^{5+} center, presumably Mo_2(A) the center adjacent to the C_5 ring. The spectra of $\mathbf{IV}^+$ are, however, much more interesting, and a comparison of the spectra of $W_2(O_2C^tBu)_4^+$, $[(^tBuCO_2)_3W_2]_2(\mu\text{-}O_2CCO_2)^+$, and $\mathbf{IV}^+$ is shown in Figure 8. The signal at g = 1.795 for $\mathbf{IV}^+$ (lower spectrum) is consistent with a metal based oxidation, with the low g value being due to extensive spin−orbit coupling.[39] The

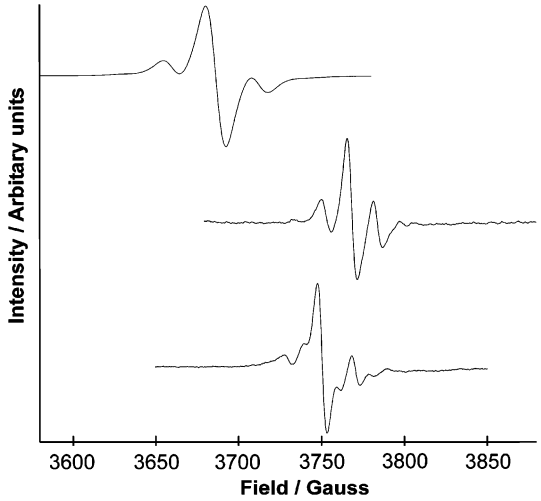

Figure 8. EPR spectra of $\mathbf{IV}^+PF_6^-$ in 2-MeTHF at 210 K (bottom), alongside those of $W_2(O_2C^tBu)_4^+PF_6^-$ (top) and $[(^tBuCO_2)_3W_2]_2(\mu\text{-}O_2CCO_2)^+PF_6^-$ (middle).

majority of tungsten nuclei have I = 0, but the ^{183}W isotope has $I = {}^1/_2$ which occurs in 14.3% natural abundance. Thus the spectrum shown for $W_2(O_2C^tBu)_4^+$ arises from the single electron on the delta orbital seeing two equivalent nuclei. The probability of both of these being ^{183}W with $I = {}^1/_2$ is very small (∼2%), so the spectrum takes on the form of a central signal flanked by satellites due to coupling to ^{183}W. The A_0 value is 51 G. For the W_4 oxalate cation $[(^tBuCO_2)_3W_2]_2(\mu\text{-}O_2CCO_2)^+$, which is known to be Class III, the single electron is delocalized over all four tungsten atoms.[24] The A_0 value due to coupling to ^{183}W (31 G) is roughly half that for $W_2(O_2C^tBu)_4^+$, and now the satellite spectrum is rather different reflecting the greater probability of a molecule having one ^{183}W and even two ^{183}W nuclei. The latter gives rise to a three-line spectrum for which only the outer lines are visible in Figure 8.

For $\mathbf{IV}^+$, the EPR spectrum is again different and may be reconciled by the presence of a single W_4^{9+} containing ion in which the single unpaired electron is delocalized over all four tungsten nuclei but in an unsymmetrical manner. The A_0 values are 20 and 41 G which is consistent with the single electron

(38) Crutchley, R. J. *Adv. Inorg. Chem.* **1994**, *41*, 273.
(39) Chisholm, M. H.; D'Acchioli, J. S.; Pate, B. D.; Patmore, N. J.; Dalal, N. S.; Zipse, D. J. *Inorg. Chem.* **2005**, *44*, 1061.

residing more on W_2(A) relative to W_2(B) as expected based on the calculated polar nature of the HOMO. See Figure 3.

Could this be a case of valence isomers[40] involving say 67% oxidation of W_2(A), i.e., valence-trapped, Class II behavior but with differing percentages of oxidation of each M_2 center? No! If this were the case, we would expect to see the signal of a W_2^{5+} ion; i.e., one akin to $W_2(O_2C^tBu)_4^+$ with $A_0 > 50$ G. The nature of the present spectrum is that corresponding to a singly occupied molecular orbital delocalized over four tungsten atoms but a greater contribution from W_2(A). We recently described a similar polarization in the heteronuclear dinuclear ion MoW-$(O_2C^tBu)_4^+$ where the δ^1 electron is polarized toward the Mo center.[39]

As discussed in our earlier work,[39,41] the asymmetry in the spectra in Figure 8 can be ascribed to the M_I dependence of the hyperfine peaks of the W nuclei so that the lower-field components are broadened. We have verified that this is the case by comparing the spectra at both Q- and X-band. At X-band they are much better resolved because the g-broadening is much less at the 4-fold lower frequencies. We have found that such comparative and predictive measurements at two different microwave frequencies are crucially important to a detailed understanding of the EPR spectra of the paramagnetic complexes with the sizes of ligands such as those in this study.

Concluding Remarks.

This work has shown that the 2,6-azulenedicarboxylate ligand is an effective bridge for coupling two M_2 quadruply bonded centers, and the following points are worthy of specific note.

1. The electronic coupling is notably greater for tungsten than for molybdenum, and this is solely an effect of the more favorable orbital energy and the greater radial extension of the W 5d orbitals. This manifests itself in the lower energy and much more intense ML(bridge)CT bands in the neutral molecule **IV** relative to **III** and in the fully delocalized nature of the radical cation $\mathbf{IV}^+$ compared to the Class II and valence-trapped $\mathbf{III}^+$.

2. These complex molecules conform well to the rather simple descriptions for strongly coupled Class III compounds presented in Schemes 1 and 2. Furthermore, in the present instance, the coupling of the two M_2 centers arises almost exclusively via electron transfer through the π^* system of the bridge (Scheme 1), via mixing of M_2 δ and bridge π^* orbitals (Scheme 2). Despite the favorable orbital energy of the bridge π-orbital, the HOMO-2 appears completely inept in facilitating hole hopping/transfer. This is evident from the lack of a low energy LMCT band in the spectrum of $\mathbf{IV}^+$ and by the fact that the HOMO-2 is a carbon-based orbital that does not mix with the M_2 δ orbitals. Furthermore, there is essentially no CO_2 π character to this orbital which further impedes any interaction with the M_2 δ^* orbitals, which in any event are energetically unfavorably disposed being notably higher in energy than the LUMO.

3. With an $M_2\cdots M_2$ distance of ~13.6 Å, the delocalized nature of the single electron in $\mathbf{IV}^+$ over four tungsten atoms is extremely rare. The low g value of 1.795, together with the nature of the hyperfine spectrum, indicates unequivocally that the oxidation is metal-centered and not bridge-based. The magnitudes of the hyperfine coupling $A_0 = 41$ and 20 G indicate that the wave function, although delocalized over both W_2 units, is polarized toward one W_2 center. Based on the calculations and a consideration of the somewhat polar nature of the bridge arising from the resonance contribution shown in **A**, we propose that the SOMO has more W_2(A) character than W_2(B).

4. Linked M_2 quadruply bonded systems offer many attractive features for the study of electronic coupling mechanisms. They are much simpler than related t_{2g}^5-bridge-t_{2g}^6 systems where several metal-based orbitals and significant spin−orbit coupling complicate the interpretation of the low energy near-IR and IR bands, of which there are several. Although the Creutz−Taube ion was prepared in 1968,[2] it was only in 1991 that it was firmly established to be Class III in nature,[38,42] and to this day, EPR spectroscopy has not been able to establish delocalization over both Ru centers.[43]

Finally, based on the principles gained from this study, we believe it will be possible to extend delocalization well beyond 14 Å by selection of a suitable bridge linking two W_2 quadruply bonded centers.

Further work is in progress.

Acknowledgment. The authors thank the National Science Foundation for support of this work and the Ohio Supercomputer Center for generous allocation of computing resources. Dr. Chistopher Hadad is thanked for assistance with DFT calculations, and Dr. Kari Green-Church is thanked for assistance in obtaining the MALDI-MS data. TCH thanks Dr. Douglas Powell for assistance with X-ray work.

Supporting Information Available: Complete description of the X-ray crystallographic work for **II**. UV/vis spectra of **I** in aq. KOH, **III** and **IV** as Nujol mulls, and the EPR spectrum of $\mathbf{III}^+PF_6^-$. Atomic coordinates for $[(HCO_2)_3M_2]_2(\mu\text{-}O_2CC_{10}H_6\text{-}CO_2)$ (M = Mo, W) and labeling scheme. This material is available free of charge via the Internet at http://pubs.acs.org.

JA0541884

(40) Salsman, J. C.; Kubiak, C. P.; Ito, T. *J. Am. Chem. Soc.* **2005**, *127*, 2382.
(41) Dalal, N. S.; Millar, J. M.; Jagadeesh, M. S.; Seehra, M. S. *J. Chem. Phys.* **1981**, *74*, 1916.
(42) Oh, D. H.; Sano, M.; Boxer, S. G. *J. Am. Chem. Soc.* **1991**, *113*, 6880.
(43) Stebler, A.; Ammeter, J. H.; Furholz, U.; Ludi, A. *Inorg. Chem.* **1984**, *23*, 2764.